Journal of Engineering Mathematics **33:** 353–376, 1998.

The manufacture of continuous smelting electrodes from carbon-paste briquettes

A. D. FITT[1] and P. D. HOWELL[2]
[1]*Faculty of Mathematical Studies, University of Southampton, SO17 1BJ, U.K.*
[2]*Mathematical Institute, 24–29 St. Giles, Oxford OX1 3LB, U.K.*

Received 25 July 1997; accepted in revised form 4 March 1998

Abstract. Continuously consumed electrodes are used in the manufacture of ferro alloys, aluminium, silicon metal and calcium carbide. The raw material for the electrodes is a carbon paste which is normally added to the electrode in large solid sections. The option of manufacturing such electrodes from small paste 'briquettes' is examined with respect to an industrial experiment used to predict the quality of a briquette-formed electrode. It is shown that successful predictive models may be formulated using a two-phase slow-flow approach. Consideration is also given to the briquette manufacture of Persson and Bruff electrodes, two different commercially important devices for the production of silicon.

Keywords: two-phase flow, viscous-dominated flow, free-boundary problems, continuous electrodes.

1. Introduction

Continuous electrodes are widely used in electric smelting furnaces. Although this technology was developed originally in the early part of this century, changes in it have been pioneered by the Norwegian company Elkem ASA who have become the acknowledged leaders in this field. The purpose of such electrodes (of which there are a number of different types – see below for further details) is to conduct currents of up to 150,000 Amps to the centre of a smelting furnace or Hall-Héroult cell, thereby providing the energy required to produce aluminium, silicon, calcium carbide or ferroalloys. A schematic diagram of the process is shown in Figure 1. (In most commercial furnaces three such electrodes are used.) During a typical process the electrodes (together with any metal casing or other sort of housing that may be present) are consumed at a rate of about 0·5 m/day and are normally charged by adding large (typically 1 m high cylinders of diameter up to 1 m) blocks of raw material to the top of the electrode. Central to the issues that will be discussed below is the raw material that makes the electrodes, which will hereafter be referred to as 'paste'. This is a mixture of binder (tar and pitch) and calcined anthracite. The anthracite particles are present in a wide size range and may have dimensions of anything between a number of microns and a few millimeters. Solid at room temperature, the paste starts to soften at around 50°C and flows when the temperature reaches 80°C. The effective viscosity of (standard Søderberg) paste reaches a minimum value at about 200–250°C, after which it increases with temperature as the anthracite particles begin to react and bind. At around 400°C the paste viscosity increases rapidly and the electrode 'bakes', becoming solid at 500°C. At 1000°C the bake is complete. During the baking the strength of the electrode is increased greatly and its thermal conductivity is improved by a factor of between two and four; the electrical conductivity is increased by orders of magnitude, so that an insulator is transformed into a conductor.

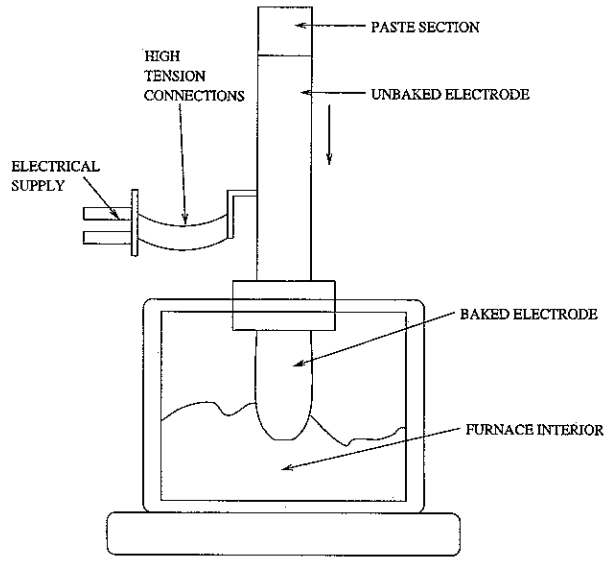

Figure 1. Schematic diagram of a typical continuous electrode smelting furnace.

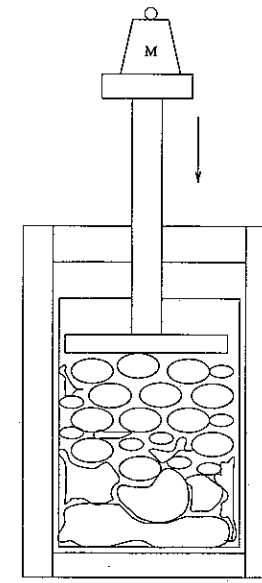

Figure 2. Experimental device for measurement of briquette density.

At present, the self-baking continuous electrode is used successfully throughout the world (for further details see [1]). One important aspect of the procedure that has been identified as an area where design improvements could be made, however, concerns the recharging of the electrode. Presently large sections are used to replenish the electrode above the furnace. Although the charging of a Søderberg electrode is a fairly easy process, for the Persson electrode (see Section 4 for a general description of this electrode) it is not possible to apply cylinders for replenishment. Only one alternative to section replacement has seriously been considered; instead of using large sections of paste for electrode replenishment, 'briquettes' (small bricks of paste of typical dimensions $10 \times 6 \times 4$ cm) may simply be added to the top of the electrode. As the briquettes gradually progress downwards towards the furnace, the increase in temperature causes them to flow, the air in the gaps between the briquettes is expelled, and a self-baking electrode is formed.

Full-scale electrodes charged with briquettes have been tested and are currently in operation; however, a great deal of further information is required concerning this new process. Some initial investigative experiments have taken place with apparatus similar to that shown in schematic in Figure 2. The piston in the device is loaded with a mass M ($M = 31$ kg in the Elkem experiments carried out so far) and the experiment takes place in a low-powered oven where the temperature is held constant at about 100°C. The piston and the sides of the container are perforated so that air can easily escape but molten paste cannot. Over a period of 5–6 hours the position of the top of the piston is monitored, allowing the effective (*i.e.* paste + air) paste density to be measured.

The main purpose of the current study is to propose models for the experiment. Although ultimately the aim is to understand the paste melting and baking processes that occur in full sized electrodes, it is anticipated that information gained from the experiment will be important in determining the details of briquette production. A good qualitative and quantitative

understanding of the experiment via mathematical modelling is therefore required. The main requirements of a theoretical approach to the problem are:

(a) that any resulting models should be predictive, but fairly simple in nature;
(b) that the important parameters in the problem should be clearly identified;
(c) that the time scales for the melting of the briquettes should be determined and;
(d) that models should possess the potential to be 'scaled up' for application to commercial electrodes.

In any mathematical study of the the experiment, two factors are immediately evident. First, the key property that must be measured and predicted is the final void fraction of the paste/air mixture after the paste melts. When subsequent baking takes place, the electrical conductivity, mechanical strength and hence the final quality of the electrode depend a great deal upon the quantity of voids that have been 'baked in'. Second, it is clear that the process involves two-phase flow, the interaction between the phases being of importance. It will transpire that many simplifications may be made to the general equations of motion; for this reason we take a rather general initial approach to the two-phase flow problem in order that the status of each simplifying step be clear.

2. Two-phase flow modelling

We begin by setting up a two-phase flow framework that will allow us to examine both the experiment and full-sized electrodes. Although subsequent simplifications will be made, the two-phase equations will be posed in some generality, so that the assumptions involved in the modelling may be clearly understood. We label the air and paste phases 1 and 2, respectively. The general picture is then of a network of pores which slowly fill with melting paste as the temperature increases and close as the paste is compressed. The three-dimensional equations of two-phase flow may then be written (see [2])

$$(\alpha_1\rho_1)_t + \nabla\cdot(\alpha_1\rho_1\boldsymbol{u}_1) = 0, \tag{1}$$

$$(\alpha_2\rho_2)_t + \nabla\cdot(\alpha_2\rho_2\boldsymbol{u}_2) = 0, \tag{2}$$

$$(\alpha_1\rho_1\boldsymbol{u}_1)_t + \nabla\cdot(\alpha_1\rho_1\boldsymbol{u}_1\boldsymbol{u}_1) = \nabla\cdot(\alpha_1(\boldsymbol{T}_1 + \boldsymbol{T}_1^{\mathrm{Re}})) + \alpha_1\rho_1\boldsymbol{g} + \boldsymbol{M}_1, \tag{3}$$

$$(\alpha_2\rho_2\boldsymbol{u}_2)_t + \nabla\cdot(\alpha_2\rho_2\boldsymbol{u}_2\boldsymbol{u}_2) = \nabla\cdot(\alpha_2(\boldsymbol{T}_2 + \boldsymbol{T}_2^{\mathrm{Re}})) + \alpha_2\rho_2\boldsymbol{g} + \boldsymbol{M}_2, \tag{4}$$

$$\begin{aligned}(\alpha_1\rho_1 e_1)_t + \nabla\cdot(\alpha_1\rho_1\boldsymbol{u}_1 e_1) \;=\; & \alpha_1\boldsymbol{T}_1\colon\nabla\boldsymbol{u}_1 - \langle\chi_1 p_1\nabla\cdot\boldsymbol{u}_1'\rangle - \nabla\cdot\alpha_1(\boldsymbol{q}_1 + \boldsymbol{q}_1^{\mathrm{Re}}) \\ & + \alpha_1\rho_1 r_1 + E_1 + \alpha_1 D_1,\end{aligned} \tag{5}$$

$$\begin{aligned}(\alpha_2\rho_2 e_2)_t + \nabla\cdot(\alpha_2\rho_2\boldsymbol{u}_2 e_2) \;=\; & \alpha_2\boldsymbol{T}_2\colon\nabla\boldsymbol{u}_2 - \langle\chi_2 p_2\nabla\cdot\boldsymbol{u}_2'\rangle - \nabla\cdot\alpha_2(\boldsymbol{q}_2 + \boldsymbol{q}_2^{\mathrm{Re}}) \\ & + \alpha_2\rho_2 r_2 + E_2 + \alpha_2 D_2.\end{aligned} \tag{6}$$

In these equations (in which it has been assumed that there is no interphase mass exchange) α represents volume fraction ($\alpha_1 + \alpha_2 = 1$), ρ and $\boldsymbol{u}$ denote density and velocity, respectively, and a prime indicates fluctuating quantities, whilst $\boldsymbol{T}$ and $\boldsymbol{T}^{\mathrm{Re}}$ denote respectively the stress

and Reynolds' stress. (Standard tensor notation has been used here so that $\boldsymbol{A}:\boldsymbol{B} = A_{ji}B_{ij}$.) The gravity vector is given by $\boldsymbol{g}$, $\boldsymbol{M}$ denotes interfacial momentum source, $\boldsymbol{q}$ and $\boldsymbol{q}^{\mathrm{Re}}$ are, respectively, the energy and turbulent energy fluxes and $\chi_i(\boldsymbol{x})$ is the phase indicator function which takes the value 1 if $\boldsymbol{x}$ is in phase i and zero otherwise. The terms E_k and D_k are, respectively, the interfacial heat source in phase k and the dissipation in phase k, whilst r denotes energy-source terms. The pressure and internal energy are given by p and e, respectively.

It is important to note that the two-phase flow equations given above (which have become the recognised starting point for models of many different two-phase flow regimes) are posed entirely in terms of *ensemble averaged* variables. Although space does not permit a full discussion of such averaging procedures (which may be carried out in many different ways; see, for example [2]), we generally define the ensemble average $\langle f\rangle$ of a field $f(\boldsymbol{x}, t)$ by

$$\langle f\rangle = \int_M f(\boldsymbol{x}, t; \xi)\,\mathrm{d}m(\xi),$$

where $m(\xi)$ is the probability of observing the result ξ and M is the set of all such results. Put crudely, this approach consists of adding the results from a number of different experimental observations and dividing by the number of observations. The details of the averaging need not concern us, but it is worth remembering that the variables in the Equations (1–6) have complicated definitions. For example, $\alpha_k = \langle\chi_k\rangle$, $\rho_k = \langle\chi_k\rho\rangle/\langle\alpha_k\rangle$ and $\boldsymbol{u}_k = \langle\chi_k\rho\,\boldsymbol{u}\rangle/\langle\chi_k\rho\rangle$. It is therefore dangerous to interpret the averaged variables in a pointwise manner so that, for example, if it transpires that a component of $\boldsymbol{u}$ is less than zero, this does not necessarily mean that all the air particles have a negative velocity.

It is now necessary to invoke closure assumptions to derive a closed model from (1–6). In the momentum equations, we assume that the Reynolds' stress terms are negligible, (subsequent estimates will show that all the relevant Reynolds numbers are small) the gravity vector is given by $\boldsymbol{g} = -g\,\boldsymbol{k}$ (where $\boldsymbol{k}$ is a unit vector in the z-direction) and that

$$\boldsymbol{T}_k = -p_k\,\boldsymbol{I} + \tau_k, \quad (\tau_k = \mu_k(\nabla\,\boldsymbol{u} + \nabla\,\boldsymbol{u}^T)),$$

where μ_k denotes the dynamic viscosity of phase k. The terms $\boldsymbol{M}_k$ represent the interfacial forces arising from stresses on the interface. It has become normal (see, for example [3]) to write

$$\boldsymbol{M}_k = p_{ki}\nabla\alpha_k + \boldsymbol{M}'_k, \quad (k = 1, 2),$$

where p_{ki} is the interfacially averaged pressure of phase k and the terms $\boldsymbol{M}'_k$ contain all forces that are related to drag, virtual mass and any other unsteady flow effects that might be important. If we ignore all such effects except for the interphase drag $\boldsymbol{D}_{ij}$ exerted on phase i due to phase j, we find that the momentum equations become

$$(\alpha_k\rho_k\,\boldsymbol{u}_k)_t + \nabla\cdot(\alpha_k\rho_k\,\boldsymbol{u}_k\,\boldsymbol{u}_k) + \alpha_k\nabla p_k = \nabla\cdot(\alpha_k\,\boldsymbol{\tau}_k) - \alpha_k\rho_k g\,\boldsymbol{k}$$

$$+ (p_{ki} - p_k)\nabla\alpha_k + \boldsymbol{D}_{kj}$$

and it now only remains to deal with the energy equations. Much modelling and discussion is required here if the job is to be done carefully and many alternatives are possible. We prefer to adopt a simple approach, assuming that the interfacial heat sources and the dissipation are

both zero (both these assumptions may have to be reviewed in some circumstances, since the chemical reactions that bake the paste may provide extra heat sources and the viscous dissipation may be nonnegligible under some circumstances). We assume (consistent with the momentum equations) that fluctuation terms may be ignored, and neglect bulk, interfacial and dissipative energy sources. Then, using the Fourier law $\boldsymbol{q}_k = -k_k \nabla T$, where T is temperature (as distinct from the tensor quantity $\boldsymbol{T}$) and k_k is the thermal conductivity of phase k, and $e_k = c_{pk} T_k$, where c_p denotes the specific heat at constant pressure, we find that the tree-dimensional ensemble-averaged two-phase flow equations may be written

$$(\alpha_1 \rho_1)_t + \nabla \cdot (\alpha_1 \rho_1 \boldsymbol{u}_1) = 0, \tag{7}$$

$$(\alpha_2 \rho_2)_t + \nabla \cdot (\alpha_2 \rho_2 \boldsymbol{u}_2) = 0, \tag{8}$$

$$\begin{aligned}(\alpha_1 \rho_1 \boldsymbol{u}_1)_t + \nabla \cdot (\alpha_1 \rho_1 \boldsymbol{u}_1 \boldsymbol{u}_1) + \alpha_1 \nabla p_1 \\ = \nabla \cdot (\alpha_1 \mu_1 (\nabla \boldsymbol{u}_1 + (\nabla \boldsymbol{u}_1)^T)) - \alpha_1 \rho_1 g \boldsymbol{k} + (p_{1i} - p_1) \nabla \alpha_1 + \boldsymbol{D}_{12},\end{aligned} \tag{9}$$

$$\begin{aligned}(\alpha_2 \rho_2 \boldsymbol{u}_2)_t + \nabla \quad (\alpha_2 \rho_2 \boldsymbol{u}_2 \boldsymbol{u}_2) + \alpha_2 \nabla p_2 \\ = \nabla \cdot (\alpha_2 \mu_2 (\nabla \boldsymbol{u}_2 + (\nabla \boldsymbol{u}_2)^T)) - \alpha_2 \rho_2 g \boldsymbol{k} + (p_{2i} - p_2) \nabla \alpha_2 + \boldsymbol{D}_{21},\end{aligned} \tag{10}$$

$$(\alpha_1 \rho_1 c_{p1} T_1)_t + \nabla \cdot (\alpha_1 \rho_1 \boldsymbol{u}_1 c_{p1} T_1) = \alpha_1 \boldsymbol{T}_1 : \nabla \boldsymbol{u}_1 + \nabla \cdot (\alpha_1 k_1 \nabla T_1), \tag{11}$$

$$(\alpha_2 \rho_2 c_{p2} T_2)_t + \nabla \cdot (\alpha_2 \rho_2 \boldsymbol{u}_2 c_{p2} T_1) = \alpha_2 \boldsymbol{T}_2 : \nabla \boldsymbol{u}_2 + \nabla \cdot (\alpha_2 k_2 \nabla T_2), \tag{12}$$

The Equations (7–12) may be thought of as the basic two-phase flow model, and we may now further simplify these using some dimensional analysis pertinent to the particular experiment that is being analysed.

We scale pressures with $\mu_2 U_2 / L_2$ and time with L_2 / U_2 where U_2 and L_2 are a typical speed and length scale in the paste flow. In the equation (10) for the paste momentum, the ratio of inertial to viscous forces is thus given by

$$\mathrm{Re}_2 = \frac{\rho_2 U_2 L_2}{\mu_2}.$$

Reasonable values for these parameters seem to be $\rho_2 \sim 1570$ kg/m^3, $U_2 \sim 1$ cm/hour and (basing the length scale on the typical dimensions of a briquette) $L_2 \sim 5$ cm, so that, even when a paste viscosity value of $\mu_2 \sim 10^4$ kg/s/m (almost certainly a gross underestimate – see later discussion on paste viscosity) is assumed, we find that

$$\mathrm{Re}_2 \sim 2 \times 10^{-8}.$$

Evidently, under normal circumstances the viscous and the pressure terms in the equation must be retained, and, since the ratio of gravity to viscous forces is given by

$$\frac{\text{gravity}_2}{\text{viscosity}_2} \sim \frac{\rho_2 g L_2^2}{\mu_2 U_2} \sim 10^7 / \mu_2$$

and μ_2 in S.I. units ranges in order of magnitude from 10^4 to 10^8, the gravity term cannot normally be neglected. As far as the interfacial pressure term (which assumes such importance in many two-phase flows) is concerned, we note that it seems likely that the bulk and interfacial pressures will be almost identical in both phases. This term is thus ignored. In the gas momentum equation, we scale p_1 with $\mu_2 U_2/L_2$, length and time with L_2 and L_2/U_2 respectively, and $\boldsymbol{u}_1$ with a typical gas velocity U_1 say. Using a typical gas viscosity $\mu_1 = 2 \times 10^{-5}$ kg/m/sec, we find that the (dimensionless) ratios of inertial to pressure force, pressure to viscous force and gravity to pressure forces are given, respectively, by

$$\frac{\text{inertia}_1}{\text{pressure}_1} \sim \frac{U_1 \rho_1 L_2}{\mu_2} \sim \frac{0{\cdot}05 U_1}{\mu_2}, \qquad \frac{\text{pressure}_1}{\text{viscous}_1} \sim \frac{\mu_2 U_2}{\mu_1 U_1} \sim \frac{5\mu_2}{36 U_1},$$

$$\frac{\text{gravity}_1}{\text{pressure}_1} \sim \frac{\rho_1 g L_2^2}{\mu_2 U_2} \sim \frac{9 \times 10^3}{\mu_2}.$$

Inertia is therefore negligible also in the gas momentum equation, gravity may be ignored and the pressure forces are many orders of magnitude larger than the viscous forces, largely as a result of the very small value of the viscosity ratio μ_1/μ_2. Surface tension is also ignored in both equations as a simple order-of-magnitude argument suggests that it will play a nontrivial role only when the pore radius is less then about 10 μm. Finally, the interfacial pressure in the gas equation is assumed to be equal to the bulk gas pressure.

The two temperature equations require some careful analysis: in the experiment the temperature range is about $\Delta T = 80°\text{C}$ and the thermal conductivity of paste varies between about 2 and 3 W/m/K. We set $T_i = T_0 + \Delta T \bar{T}_i$ (where T_0 is a typical reference temperature), $p_i = \mu_2 U_2 \bar{p}_i / L_2$, $\boldsymbol{x} = L_2 \bar{\boldsymbol{x}}$, $\boldsymbol{u}_i = U_2 \bar{\boldsymbol{u}}_i$ and $t = L_2 \bar{t}/U_2$ and find, on dropping the bars and simplifying, that

$$\begin{aligned}(\alpha_1 \rho_1 c_{p1} T_1)_t + \nabla \cdot (\alpha_1 \rho_1 c_{p1} \boldsymbol{u}_1 T_1) \\ = -\frac{U_2}{\Delta T L_2} \alpha_1 p_1 \mu_2 \nabla \cdot \boldsymbol{u}_1 + \frac{U_2}{\Delta T L_2} \alpha_1 \mu_1 \left(\frac{\partial u_{1i}}{\partial x_j} + \frac{\partial u_{1j}}{\partial x_i} \right) \frac{\partial u_{1i}}{\partial x_j} \\ + \frac{1}{L_2 U_2} \nabla \cdot (\alpha_1 k_1 \nabla T_1),\end{aligned} \tag{13}$$

$$\begin{aligned}(\alpha_2 \rho_2 c_{p2} T_2)_t + \nabla \cdot (\alpha_2 \rho_2 c_{p2} \boldsymbol{u}_2 T_2) \\ = -\frac{U_2}{\Delta T L_2} \alpha_2 p_2 \mu_2 \nabla \cdot \boldsymbol{u}_2 + \frac{U_2}{\Delta T L_2} \alpha_2 \mu_2 \left(\frac{\partial u_{2i}}{\partial x_j} + \frac{\partial u_{2j}}{\partial x_i} \right) \frac{\partial u_{2i}}{\partial x_j} \\ + \frac{1}{L_2 U_2} \nabla \cdot (\alpha_2 k_2 \nabla T_2).\end{aligned} \tag{14}$$

Using the typical values $\rho_1 \sim 1$ kg/m^3, $c_{p1} \sim 10^3$ J/kg/k, $k_1 \sim 3 \times 10^{-2}$ W/m/K, along with $U_2 \sim 2{\cdot}8 \times 10^{-6}$ m/s and $L_2 \sim 0{\cdot}05$ m as before, we find that the terms on the left-hand side of (13) are about 10^3, whilst the first two terms on the right-hand side have orders of magnitude $7 \times 10^{-7} \mu_2$ and $7 \times 10^{-7} \mu_1$, respectively. Finally, the diffusion term is about 2×10^5. The diffusion term is therefore dominant for physically realistic values of the viscosity. In (14), the conclusions are similar when typical values of $c_{p2} \sim 900$ J/kg/K, $k_2 \sim 2{\cdot}5$ W/m/K are used,

the only difference being that now the left-hand side is comparable to the diffusion term and must be retained.

Finally, assuming that the densities in both phases are constant (the densities and thermal properties all change by small amounts over the the temperature ranges that are to be considered; these effects could be included if required) and writing for simplicity $\alpha_2 = \alpha$, $\alpha_1 = 1-\alpha$ and $\boldsymbol{D} = \boldsymbol{D}_{21} = -\boldsymbol{D}_{12}$, we find that the two-phase flow equations reduce to

$$\alpha_t + \nabla \cdot (\alpha \boldsymbol{u}_2) = 0, \tag{15}$$

$$-\alpha_t + \nabla \cdot ((1-\alpha)\boldsymbol{u}_1) = 0, \tag{16}$$

$$\alpha \nabla p_2 = \nabla \cdot (\alpha \mu_2 [\nabla \boldsymbol{u}_2 + (\nabla \boldsymbol{u}_2)^T]) - \rho_2 \alpha g \boldsymbol{k} + \boldsymbol{D}, \tag{17}$$

$$(1-\alpha)\nabla p_1 = -\boldsymbol{D}, \tag{18}$$

$$0 = \nabla \cdot ((1-\alpha) k_1 \nabla T_1), \tag{19}$$

$$(\alpha \rho_2 c_{p2} T_2)_t + \nabla \cdot (\alpha \rho_2 c_{p2} \boldsymbol{u}_2 T_2) = \nabla \cdot (\alpha k_2 \nabla T_2). \tag{20}$$

The Equations (15–20) will form the basis of models for both the Elkem experiment and real electrodes. We note immediately that the system is not closed, since it involves more unknowns than there are equations. To close the system we need a constitutive relation for the interactive drag $\boldsymbol{D}$, and a relation between p_1 and p_2. We make the simplifying assumption $p_1 = p_2$. Although for inertia-dominated flows setting the phasic pressures equal to each other may be dangerous and lead to ill-posed problems, (see, for example [4]), for flows where the viscosity is dominant it is known that this is normally a reasonable assumption. (Controversy rages about the correct closure condition for two-phase flows, but it has become common practice to set $p_1 = p_2$ in the absence of any conclusive evidence to the contrary.) For the drag $\boldsymbol{D}$ we observe the following scalings. If

$$\boldsymbol{u}_2 \sim U_2, \qquad \boldsymbol{x} \sim L_2,$$

then

$$\boldsymbol{u}_1 \sim U_1 \sim \frac{\alpha U_2}{1-\alpha}, \qquad p_{1,2} \sim \frac{\mu_2 U_2}{L_2},$$

and assuming Poiseuille/Stokes drag,

$$\boldsymbol{D} \sim \frac{\alpha \mu_1 \boldsymbol{u}_1}{R^2},$$

where R is a typical pore radius. Hence, after nondimensionalisation (18) reads

$$\nabla p_1 \sim \frac{\mu_1}{\mu_2} \cdot \frac{L_2^2}{R^2} \cdot \frac{\alpha^2}{(1-\alpha)^2}. \tag{21}$$

Since $\mu_1/\mu_2 < O(10^{-10})$, we can take

$$p_1 = \text{const.} \tag{22}$$

at least until the pores shrink to the point that $R(1-\alpha)/L_2 \sim 10^{-5}$. Hence in this regime, (hereafter referred to as '*Regime I*') we obtain a closed system for α, $\boldsymbol{u}_2$ and T_2 in the form

$$\alpha_t + \nabla \cdot (\alpha \boldsymbol{u}_2) = 0, \tag{23}$$

$$\nabla \cdot (\alpha \mu_2 [\nabla \boldsymbol{u}_2 + (\nabla \boldsymbol{u}_2)^T]) = \rho_2 \alpha g \boldsymbol{k}, \tag{24}$$

$$(\alpha \rho_2 c_{p2} T_2)_t + \nabla \cdot (\alpha \rho_2 c_{p2} \boldsymbol{u}_2 T_2) = \nabla \cdot (\alpha k_2 \nabla T_2). \tag{25}$$

(Once (23–25) have been solved, $\boldsymbol{u}_1$ and T_1 may be calculated if required from (16) and (19).)

The above model may not hold for all stages of the process, since it allows α to increase indefinitely. In practice, when α reaches some critical value, α_c say, the pores close off to form isolated packets or bubbles of air. Once this has occurred, α cannot change, since the air is unable to escape, and the problem reduces to

$$\alpha = \alpha_c, \tag{26}$$

$$\nabla \cdot \boldsymbol{u}_2 = 0, \tag{27}$$

$$\nabla p_2 = \alpha_c \nabla \cdot (\mu_2 [\nabla \boldsymbol{u}_2 + (\nabla \boldsymbol{u}_2)^T]) - \rho_2 \alpha_c g \boldsymbol{k}, \tag{28}$$

$$(\rho_2 c_{p2} T_2)_t + \nabla \cdot (\rho_2 c_{p2} \boldsymbol{u}_2 T_2) = \nabla \cdot (k_2 \nabla T_2). \tag{29}$$

We denote this regime by *Regime II*.

The transition between regimes I and II is complicated and unlikely to be easy to analyse. We therefore neglect the details of the transition and simply assert that Regime I applies whenever $\alpha < \alpha_c$, and switch to Regime II as soon as α reaches α_c.

Some of the physical assumptions inherent in (23)–(25) and (26)–(29) merit further brief discussion. In particular, we note that, though the briquettes are in mutual contact and are contained within an external vessel, the model reflects the fact that the liquid phase is quite unable to support a pressure gradient. In contrast to the familiar case say of a single phase fluid occupying a container and subject to a pressure gradient (hydrostatic, for example) but at rest everywhere, the internal air gaps present do not permit a solution with a non-trivial pressure gradient and zero velocity. Of course, when regime II is reached and the air gaps close off to form isolated pores, the physical nature of the mixture is changed; now a pressure gradient can be supported and a hydrostatic pressure solution with zero velocity is possible. Finally, it is worth adding that many refinements could be made to the basic model: for example, the current assumption that the air and paste pressures are equal everywhere on the paste/air interface could be replaced by the more accurate condition that the normal stress is continuous. Submodels would then have to be developed to characterise the dependence of pressure upon interface geometry. Related more detailed submodelling could also be used to allow the critical void fraction α_c to be predicted rather than regarded as known; if more experimental information concerning the pore geometry becomes available, then this will be pursued.

3. Analysis of the experiment

In the Elkem experiment, a cylinder of radius a (= 8·5 cm) is filled with paste briquettes, with an initial paste fraction α_0 (= 0·45), up to an initial height L (=30 cm). A mass M (=31 kg) is

then loaded onto the top of the piston and the cylinder is heated to $T_f = 100°C$. As air is forced out by the weight of the loaded piston and of the paste itself, the mass moves downwards. Its position is plotted against time, and from this the average density of the air/paste mixture is deduced. It is observed that the density calculated by this method asymptotes to around 1430 kg/m^3, whereas the density of raw paste at such temperatures is about 1570 kg/m^3. The final density is thus about 91% of that of pure paste; this corresponds to α_c referred to earlier and we shall thus take $\alpha_c = 0{\cdot}91$ in all numerical results given below. It might be argued that 'predictions' of the experimental data should not use this result as it comes itself from the experiment: however, it is a parameter that is likely to be a property of the paste itself rather than the experiment. We therfore regard α_c as a 'known paste property'.

3.1. The full problem

Clearly the full problem, governed by (23)–(29) is a formidable one. Not only must coupled partial differential equations be solved, but either one of two regimes may be present. Since our main aim in this study is to acquire a qualitative understanding of the process, we consider some obvious simplifications, rather than embark on a full numerical study of the problem.

3.2. One-dimensional isothermal model

The simplest approach is to model the flow in the experiment as one-dimensional, with the fluid velocity $\boldsymbol{u}_2 = w(z,t)\boldsymbol{k}$. We first consider the isothermal case in which the paste has constant viscosity μ_2 and so the temperature variations in the experiment are irrelevant for the purposes of effective mixture density calculation. We nondimensionalise using

$$z = L\tilde{z}, \qquad s = L\tilde{s}, \qquad w = \frac{MgL}{2\pi a^2\mu_2}\tilde{w}, \qquad t = \frac{2\pi a^2\mu_2}{Mg}\tilde{t}, \tag{30}$$

where the moving top of the experiment (*i.e.* the bottom surface of the piston) is denoted by $z = s(t)$. The Equations (23–24) become (dropping tildes)

$$\alpha_t + (\alpha w)_z = 0, \qquad (\alpha w_z)_z = g^*\alpha. \tag{31}$$

Here

$$g^* = \frac{\pi a^2\rho_2 L}{M} \tag{32}$$

measures the relative importance of the weight of the briquettes themselves compared to that of M.

The origin for z is chosen to be the bottom of the cylinder. The initial condition for (31) is that the void fraction is specified at $t = 0$ when moving top of the experiment is at $s = 1$. We must also have $w = 0$ on $z = 0$. To determine the unknown boundary $s(t)$ evidently we must have $w = \dot{s}$ when $z = s$. In addition to this, the load is known. Since the effect of the load is communicated to the briquette column by the briquettes themselves, the (dimensional) pressure on the moving top is

$$-\frac{Mg}{\alpha\pi a^2}.$$

This must equal $2\mu_2 w_z$, and the final (non-dimensional) boundary conditions thus become

$$\begin{aligned} &\alpha = \alpha_0, \quad t = 0, \\ &w = 0, \quad z = 0, \\ &\alpha w_z = -1, \quad w = \dot{s}, \quad z = s, \\ &s = 1, \quad t = 0. \end{aligned} \tag{33}$$

The unsteady, nonlinear free-boundary problem (31), (33) may be solved explicitly, (see Appendix), giving

$$\alpha = [\alpha_0(1 + g^*t) + t]\,\mathrm{e}^{-g^*zt},$$

$$w = \frac{\alpha_0(\mathrm{e}^{g^*zt} - 1)}{g^{*}t^2[\alpha_0(1 + g^*t) + t]} - \frac{z}{t}, \qquad s = \frac{1}{g^*t}\log\left(\frac{\alpha_0(1 + g^*t) + t}{\alpha_0 + t}\right). \tag{34}$$

As noted in Section 2, this solution must eventually become invalid. (For example, when $z = 0$ the void fraction α increases indefinitely.) hence there is a shift to regime II when α reaches α_c, which occurs first at $z = 0$, $t = t_c$, where

$$t_c = \frac{\alpha_c - \alpha_0}{1 + \alpha_0 g^*}.$$

For $t > t_c$ we introduce a second free boundary $z = l(t)$ such that we have Regime I in $z > l$ and Regime II in $z < l$. The new free-boundary problem that results is (31) in $l < z \leqslant s$, with the additional boundary conditions

$$\begin{aligned} &\alpha = \alpha_c, \quad z = l, \\ &w = 0, \quad z = l, \\ &\alpha w_z = -1, w = \dot{s}, \quad z = s, \\ &l = 0, \quad t = t_c. \end{aligned} \tag{35}$$

This problem can also be solved in closed form, giving

$$\begin{aligned} \alpha &= \alpha_c \exp\left(\frac{\alpha_0 - \alpha_c + (1 + \alpha_0 g^*)t - \alpha_c g^* zt}{\alpha_c}\right), \\ w &= \frac{1 + \alpha_0 g^*}{\alpha_c g^* t} - \frac{1}{g^{*}t^2} - \frac{z}{t} + \frac{\alpha_0}{\alpha_c g^{*}t^2}\exp\left(\frac{\alpha_c - \alpha_0 - (1 + \alpha_0 g^*)t - \alpha_c g^* zt}{\alpha_c}\right), \\ s &= \frac{1 + \alpha_0 g^*}{\alpha_c g^*} - \frac{\alpha_c - \alpha_0}{\alpha_c g^* t} + \frac{1}{g^* t}\log\left(\frac{\alpha_c}{\alpha_0 + t}\right), \\ l &= \frac{(1 + \alpha_0 g^*)(t - t_c)}{\alpha_c g^* t}. \end{aligned} \tag{36}$$

Notice that after time $t_f = \alpha_c - \alpha_0$, we have $s = l$. At this point $\alpha = \alpha_c$ everywhere and the process stops.

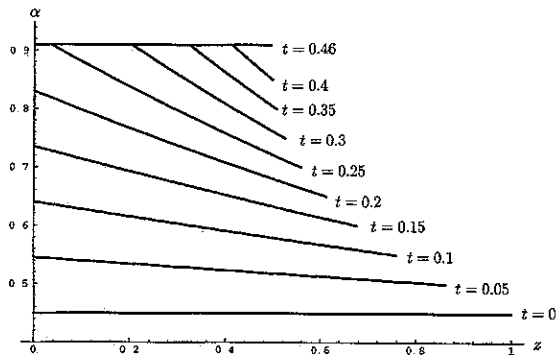

Figure 3. Paste volume fraction α versus height z for increasing values of time t. Here $g^* = 2, \alpha_0 = 0{\cdot}45$, $\alpha_c = 0{\cdot}91$

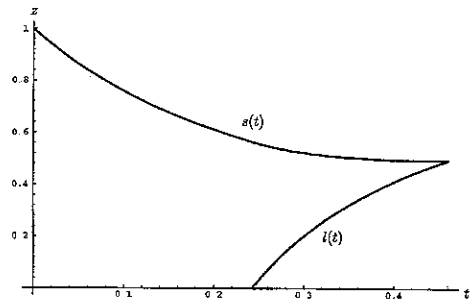

Figure 4. Free boundaries $z = s(t)$ and $z = l(t)$ versus time t. Here $g^* = 2, \alpha_0 = 0{\cdot}45, \alpha_c = 0{\cdot}91$.

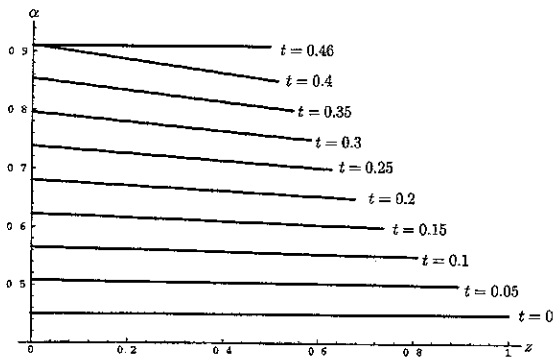

Figure 5. Paste volume fraction α versus height z for increasing values of time t. Here $g^* = 0{\cdot}34, \alpha_0 = 0{\cdot}45, \alpha_c = 0{\cdot}91$.

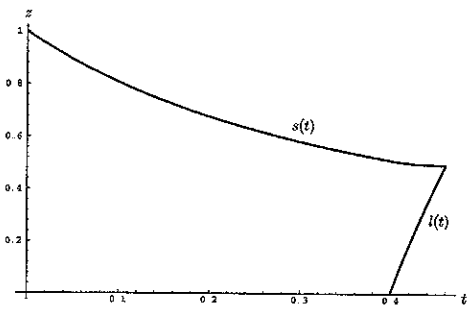

Figure 6. Free boundaries $z = s(t)$ and $z = l(t)$ versus time t. Here $g^* = 0{\cdot}34, \alpha_0 = 0{\cdot}45, \alpha_c = 0{\cdot}91$

In Figure 3 we have plotted the void fraction α against z for increasing values of t, using the parameters $g^* = 2, \alpha_0 = 0{\cdot}45$ and $\alpha_c = 0{\cdot}91$. With these values $t_c = 0{\cdot}242$, and indeed for $t > 0{\cdot}242$, we observe a region near $z = 0$ in which $\alpha = \alpha_c$. The process stops with $\alpha \equiv \alpha_c$ everywhere after time $\alpha_c - \alpha_0 = 0{\cdot}46$. The two free boundaries $s(t)$ and $l(t)$ are plotted against t in Figure 4 for the same parameter regime.

Although the behaviour for $g^* = 2$ illustrates the general features of the free-boundary movement well, for the experiment g^* is actually about 0·34. Physically this means that the mass M is about three times heavier than the paste itself. We plot α against z in Figure 5 and s and l against t in Figure 6 for this parameter regime. With this fairly small value of g^*, α remains nearly spatially uniform as t increases. A consequence of this is that $t_c = 0{\cdot}399$ and the final time $\alpha_c - \alpha_0 = 0{\cdot}46$ are nearly equal, and so the free boundary l rises very rapidly to meet s. This suggests that, under experimental conditions where heavily loaded pistons are used, we obtain a reasonable approximation by setting $g^* = 0$. This simplifies the problem considerably, since $l(t)$ may then be neglected completely.

3.2.1. *Temperature-dependent viscosity*

The analysis carried out thus far might be expected to apply to the final stages of the experiment, when the temperature, and hence the viscosity, of the paste has become uniform. Alter-

natively, it may be regarded as relevant to an experiment where the briquettes are 'preheated' to the oven temperature before they are squashed by the piston. If the Elkem experiment is to be properly simulated, however, then account must be taken of initial stages, where changes in viscosity of the slowly heated paste are important. In general, we expect that both the temperature and the paste fraction will be functions r and z, but this complicates matters to the extent that a purely numerical solution is required. Great simplifications occur, however, if we assume that the cylinder is heated uniformly and insulated at its top and bottom, and infer from this that the temperature is independent of z. (Since the motion of the paste depends upon the temperature through the viscosity, it cannot be the case that the temperature depends only on r, whilst the paste fraction depends only upon z. We nevertheless proceed under these assumptions, ignoring that fact that it will not be possible to impose the full no-slip condition on the boundary of the experimental cylinder.) Averaging across the cross-section to obtain a one-dimensional model as before, we obtain

$$\alpha_t + (\alpha w)_z = 0, \qquad \bar{\mu}_2(\alpha w_z)_z = g^*\alpha, \tag{37}$$

where $\bar{\mu}_2$ is a function only of t. A typical value of the paste viscosity, $\mathcal{M}_2$, say, is used to nondimensionalise $\bar{\mu}_2$, and in the nondimensionalisation *ansatz* (30) for w and t. The boundary conditions are

$$\begin{aligned} &\alpha = \alpha_0, \quad t = 0, \\ &w = 0, \quad z = 0, \\ &\bar{\mu}_2(t)\alpha w_z = -1, \quad w = \dot{s}, \quad z = s, \\ &s = 1, \quad t = 0. \end{aligned} \tag{38}$$

Using the methods described in the Appendix, we first solve (37) with boundary conditions (38) to yield

$$\alpha = (\alpha_0 + (1 + \alpha_0 g^*)F)\,\exp(-g^* F z),$$

$$w = \frac{\alpha_0 \dot{F}(\exp(g^* F z) - 1)}{g^* F^2(\alpha_0 + (1 + g^*\alpha_0)F)} - \frac{\dot{F} z}{F}, \qquad s = \frac{1}{g^* F}\log\left(\frac{\alpha_0 + (1 + g^*\alpha_0)F}{\alpha_0 + F}\right), \tag{39}$$

where now

$$F(t) = \int_0^t \frac{\mathrm{d}t'}{\bar{\mu}_2(t')}$$

and g^* is as defined previously in (32). This solution is valid only until α reaches α_c, which happens first at $z = 0, t = t_c$ where

$$F(t_c) = \frac{\alpha_c - \alpha_0}{1 + \alpha_0 g^*}.$$

For $t > t_c$ we need to introduce another free boundary and solve (37) in the region $l(t) < z < s(t)$ with the boundary conditions

$$\alpha = \alpha_c, \quad z = l(t),$$

$$w = 0, \quad z = l(t),$$

$$\bar{\mu}_2(t)\alpha w_z = -1, \quad w = \dot{s}, \quad z = s,$$

$$l = 0, \quad t = t_c.$$

The solution is given by

$$\alpha = \alpha_c \exp\left(\frac{(1 + g^*\alpha_0)F + \alpha_0 - \alpha_c}{\alpha_c} - g^*Fz\right),$$

$$w = \frac{\dot{F}}{g^*F^2}\left(\log\left(\frac{\alpha}{\alpha_c}\right) + \alpha_0\left(\frac{1}{\alpha} - \frac{1}{\alpha_c}\right)\right),$$

$$s = \frac{1}{g^*\alpha_c}\left(1 + g^*\alpha_0 - \frac{\alpha_c - \alpha_0}{F} + \frac{\alpha_c}{F}\log\left(\frac{\alpha_c}{\alpha_0 + F}\right)\right),$$

$$l = \frac{1}{g^*\alpha_c}\left(1 + g^*\alpha_0 - \frac{\alpha_c - \alpha_0}{F}\right). \tag{40}$$

The whole process stops with $\alpha = \alpha_c$ and $w = 0$ everywhere when $t = t_f$ where

$$F(t_f) = \alpha_c - \alpha_0.$$

As noted above, there may be future interest in conducting experiments with a heavier piston. Under circumstances when the right-hand side of the second equation of (37) may be neglected, (37) with boundary conditions (38) has the particularly simple solution

$$\alpha = \alpha_0 + F(t), \qquad w = -\frac{\dot{F}z}{\alpha_0 + F}, \qquad s = \frac{\alpha_0}{\alpha_0 + F(t)}.$$

Now that gravity has been neglected in the momentum equation, α remains spatially uniform. Thus when α reaches α_c, it does so over the whole cylinder simultaneously. This simplifies matters greatly as a second free boundary does not have to be introduced.

To make realistic comparisons with experimental data, all that remains to be determined is $\bar{\mu}_2(t)$. To do this we must consider the heat flow into the cylinder.

3.3. Heat flow

To determine the paste viscosity as the experiment progresses, we must solve (25). Normally this will give rise to a convection-diffusion equation that must be solved numerically. However, under the assumptions discussed above (namely that the cylinder is heated uniformly and insulated at its top and bottom, so that the temperature is independent of z, whilst the flow is one-dimensional) the problem may be solved in closed form. We have (assuming that the density, thermal conductivity and specific heat are constant)

$$(\alpha T_2)_t + \nabla \cdot (\alpha w \boldsymbol{k} T_2) = \frac{k_2}{\rho_2 c_{p2}} \nabla \cdot (\alpha \nabla T_2) \tag{41}$$

and thus

$$T_{2t} = \frac{k_2}{\rho_2 c_{p2}} \frac{1}{r}(rT_{2r})_r$$

with boundary conditions

$$T_2 = T_0 \quad \text{at } t = 0, \qquad T_{2r} = h(T_2 - T_f) \quad \text{on } r = a, \tag{42}$$

where h is a heat-transfer coefficient (dimensions /m) which will depend on the type of convection (for example, whether fans are used or natural convection dominates) present in the oven. In the experiment, the diameter of the cylinder is 17 cm and thus $a = 8{\cdot}5$ cm. Taking T_0 to be room temperature (say 20°C) and T_f as the oven temperature 100°C, we nondimensionalise as follows

$$r = a\tilde{r}, \qquad t = \frac{\rho_2 c_{p2} a^2}{k_2}\tilde{t}, \qquad T_2 = T_f + (T_0 - T_f)\tilde{T}, \tag{43}$$

so that the problem becomes, on dropping the tildes,

$$T_t = T_{rr} + \frac{T_r}{r}, \quad T = 1 \quad \text{at } t = 0, \quad T_r = HT \quad \text{on } r = 1, \tag{44}$$

where $H = ah < 0$. The thermal conductivity and specific heat of raw paste are given in [1] as $k_2 = 2{\cdot}5$ W/m/K and $c_{p2} = 900$ J/kg/K, respectively. If a raw paste density of 1570 kg/m^3 is used, the time scale implied by (43) is thus about 1·1 hours. We note first that this seems well in line with the experimental results and, second, that it is not possible to simplify the equations further by making the heat-flow problem quasi-steady.

The solution of (44) is

$$T = \sum_{k=0}^{\infty} \frac{-2H J_0(rp_k)\, \mathrm{e}^{-p_k^2 t}}{(H^2 + p_k^2) J_0(p_k)}, \tag{45}$$

where $p_k (k = 0, 1, 2 \ldots)$ are the zeroes of

$$pJ_1(p) + HJ_0(p) = 0.$$

When H is small (the values of most practical interest), the first root is given by

$$p_0 \sim \sqrt{-2H} - \frac{\sqrt{2}}{8}(-H)^{3/2} + \frac{5\sqrt{2}}{384}(-H)^{5/2} + O((-H)^{7/2}), \quad (H \to 0).$$

For large k, the roots are distributed according to

$$p_k \sim \pi(k + 1/4) - \frac{(3 + 8H)}{8\pi k} + \frac{(3 + 8H)}{32\pi k^2} + O(k^{-3}),$$

an approximation that gives remarkably good results, even for modest values of k. (Two-decimal-place accuracy is obtained, even when $k = 1$ for say $H = -1$.) The temperature may now be averaged across a cross-section, giving

$$\langle T \rangle = 2\int_0^1 Tr \, \mathrm{d}r = \sum_{k=0}^{\infty} \frac{4H^2 \, \mathrm{e}^{-p_k^2 t}}{p_k^2 (H^2 + p_k^2)} \tag{46}$$

so that in dimensional variables

$$\langle T \rangle = T_f + (T_0 - T_f) \sum_{k=0}^{\infty} \frac{4a^2h^2}{p_k^2(a^2h^2 + p_k^2)} \exp\left(-\frac{p_k^2 k_2 t}{\rho_2 c_{p2} a^2}\right). \tag{47}$$

Now that the temperature has been determined, we must give some thought to the viscosity that will be used to predict the experimental results. Paste viscosity was measured for a range of thermal conditions by Tørklep [5]. Using his results and after discussion with Elkem, we feel that a good approximation for paste viscosity at temperatures between 50 and 150°C is given by an Arrhenius-type law. An extra complication arises as to the exact nature of the constants appearing in the Arrhenius law, for the viscosity of the paste used in the Elkem experiment is at present proprietary information. All that may be assumed is that the paste has a viscosity of 10^4 Pa s at 150°C and is 'similar to anode paste, but less temperature dependent'. In normal circumstances the viscosity of paste depends quite strongly on the amount of coke contained in the paste, but, using the given (incomplete) data in conjunction with Tørklep's results, we propose a paste viscosity law given by

$$\mu_2 = 0{\cdot}80081 \times 10^{-6} \exp\left(\frac{9834}{T}\right), \tag{48}$$

where μ_2 is given in Pa s and the temperature in Kelvin. This formula assumes that the viscosity at 75°C is $1{\cdot}5 \times 10^6$ Pa s (a result that may be in error, but is at least roughly correct) and thus predicts a viscosity of 225071·6 Pa s at the experimental steady state temperature of 100°C, as well as a viscosity of 10^4 Pa s at 150°C. Obviously this formula should be treated as approximate and may require updating if fuller details of the paste viscosity are revealed.

3.4. Comparisons with experimental results

In order to compare with the tests performed at Elkem, the height of the piston during the experiment must be related to the effective density of the paste/air mixture. We define the mixture density ρ_m by

$$\rho_m = \alpha\rho_2 + (1 - \alpha)\rho_1 \tag{49}$$

and note that, since the amount of paste in the experimental apparatus is conserved (unlike the air, which escapes during the experiment), we have, when the piston is at a height s,

$$\int_0^s \rho_2 \alpha = C$$

where C is constant. Consideration of the conditions at the start of the experiment now shows that $C = L\rho_2\alpha_0$. Integrating (49) between 0 and s and assuming that ρ_m is constant in space, we then have

$$\rho_m = \rho_1 + \frac{L\alpha_0}{s}(\rho_2 - \rho_1).$$

Since in the experiment being analysed ρ_1/ρ_2 is less than 10^{-3}, we simply use

$$\rho_m = \frac{L\alpha_0\rho_2}{s} \tag{50}$$

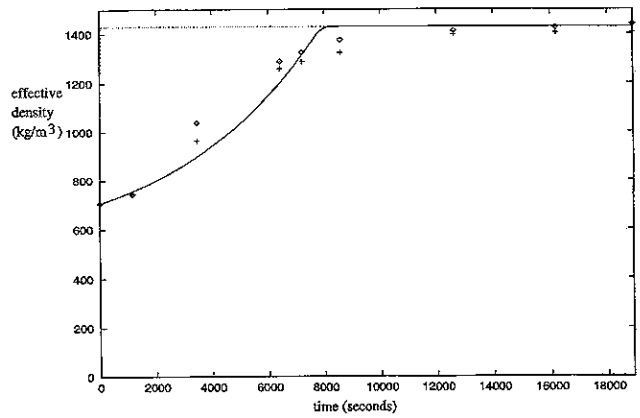

Figure 7 Comparison between theory and experimental data (symbols); constant viscosity (dashed line), temperature-dependent viscosity (solid line).

for comparison purposes.

Figure 7 shows comparisons between theoretical and experimental results. The symbols denote the results from two experiments, the density having been inferred from the position of the piston using (50). We have plotted the broken line, using the constant-viscosity one-dimensional model, the viscosity at 100°C (see above) having been used. As expected, the rise is much too sharp in comparison with the experimental results. We have plotted the solid line, using (47), (39) and (40); the heat-transfer coefficient used in (44) was taken to $H = -0{\cdot}05$ (at the lower end of the range suggested by Kakac and Yener [6], and in line with other quoted values) and the relevant values of t_c and t_f were 7624 and 8231 seconds, respectively, showing that regime II persists for only a relatively short time in this case (a result consistent with the conclusions of Figures 5 and 6). The inclusion of the slower rise in temperature gives results that are in much better agreement with the experimental data and shows that, as might be expected, variations in viscosity must be taken into account if accurate predictions are required. Allowing for the variations in the experimental data and the uncertainties concerning the viscosity discussed above, we conclude that the model is performing well. Agreement is not perfect, however. There are a number of possible reasons for this, apart from the sensitivity of (48) mentioned above. These include

- The thermal conductivity of paste has been used. In the early stages of the process the experimental apparatus also contains some air, which has a much lower thermal conductivity. Averages should really be used for the thermal conductivity (and possibly other thermal variables as well).
- For simplicity it has been assumed that the temperature in the experiment is determined by (37). As noted in Section 2, more consideration of the role of the pressure terms in the energy equation may be required.
- It is not absolutely clear how the experiment is begun. If the oven is switched on at the start of the process, then presumably some heating time is required before a uniform temperature is reached.
- It may be unrealistic to assume that the ends of the experimental apparatus are thermally insulated.

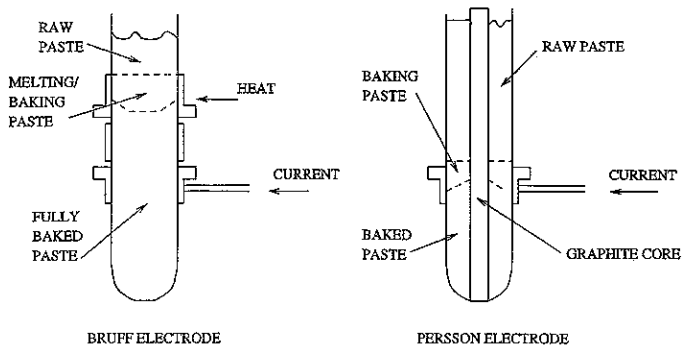

Figure 8. Schematic details of Persson and Bruff electrode designs.

- There is an inherent assumption in the model that, although the temperature varies with r and not with z, the void fraction of paste varies with z, but not with r. This is obviously unrealistic.

4. Alternative electrodes for silicon production

Although the main aim of this study is to examine the paste melting experiment, it is also valuable to consider briefly how the theory may be applied to a range of full-scale electrodes. Although detailed calculations will inevitably be of a numerical nature, we seek to establish the key parameters and time scales for a range of industrial electrodes.

Since the early part of this century, the Søderberg electrode has been the only continuous self-baking electrode available for calcium carbide and ferroalloy production. Although many technical advances have taken place to allow increases in size and efficiency, the basic design has remained almost unchanged since the first Søderberg electrode was used in 1919. For processes (manufacture of calcium carbide, ferroalloys, for instance) where the product may contain some iron, there is still no alternative to the Søderberg electrode. The fins and casing of the electrode typically introduce some 0·1–1·0% iron into the end product. If silicon were to be the end product, then about 1% iron would be introduced, an unacceptably high level Until recently, therefore, the only possibility was to use a conventional pre-baked electrode element. In recent years, however, a number of new types of electrode have been proposed with silicon production in mind. Two new designs that have attracted particular interest have become known, after their originators, as the 'Persson' and 'Bruff' electrodes.

In the Persson design, a central graphite carbon core is surrounded by paste in a stationary casing. A set of supports holds the core section in place and allows it to slip. During processing, the core is fused into the paste as it is carbonised. The great advantage of this design is that, unlike the Søderberg system where the metal electrode casing is present during the whole process and is consumed in the furnace together with the electrode, here the emerging carbon has no case This is crucial for the production of silicon where the presence and subsequent consumption of the metal electrode casing might otherwise introduce too much iron into the furnace.

The Bruff electrode uses a specialised heating zone to melt and bake the paste. Heat is provided by propane burners and some of hydrocarbons that escape from the baking paste are also used to power the process Once again, the main purpose of this arrangement is to produce a caseless electrode.

Space does not permit a full description of the details and advantages of these new types of electrode, but more information may be found in [7] and [8] where many additional advantages are claimed for the new designs. Figure 8 gives schematic details of both electrodes.

For both electrodes, the questions that must be answered are similar to those relevant to the experiment. For example, is it possible to identify circumstances under which too much air will be 'baked in' to the final product? Also, what are the requirements in terms of time or electrode length for the proper outflow of briquettes?

5. The Persson electrode

5.1. THE FULL PROBLEM

Using the theory developed above, we may propose equations for the full problem in a Persson electrode. Three separate regions have to be included, for as well as the graphite core a 'baking' and a 'baked' region must be introduced for different paste conditions. As well as the temperature, the paste velocity, void fraction and electric potential must be determined. For the sort of Persson electrode currently in use, we obtain an unsteady two-dimensional cylindrically symmetric problem. (For full details see [9].) Though complicated, the resulting equations are not nearly so formidable to solve numerically as the full two-phase flow/heating problem that would have resulted if the simplifications detailed above had not taken place. If the development of a sophisticated predictive tool was required for the analysis of Persson electrode paste melting and baking, then it seems likely that a model similar to this could be used. For the present, however, we do not consider this full model further, but content ourselves with analysing some simplified cases.

5.2. TIME SCALES FOR AIR EXPULSION IN THE ELECTRODE

From the models already developed it is clear how the time scale for paste melting and baking in the Persson electrode may be determined. The time t_c for pore closure is given essentially by a balance between gravity and viscosity, so that

$$t_C \sim \sqrt{\frac{\mu_2}{\rho_2 g U}}.$$

This corresponds to a distance down the electrode of

$$L_C \sim \sqrt{\frac{\mu_2 U}{\rho_2 g}}.$$

If $U = 0{\cdot}5$ m/day $\approx 6 \times 10^{-6}$ m/s, $\rho_2 \approx 10^3$ kg/m^3 and $\mu_2 \approx 10^n$ Pa s (the exponent n varying say between 3 and 8 to allow for temperature dependence) then

$$L_C \sim 10^{n/2-5} m.$$

Hence so long as $\mu_2 < 10^{10}$ Pa s, (almost certainly the case in practice) all the air that is going to escape will do so within about 1 metre. This indicates that regime II applies everywhere except in a small region near to the top of the electrode. This result is in stark contrast to the

experiment where regime I is normally the dominant one. One way of interpreting this result is to conclude that the experiment could be made more practically relevant by increasing the value of g^*. Indeed, it is possible that 'scaling up' results of this short may turn out to be the most important modelling conclusions from a practical point of view.

5.3. ONE-DIMENSIONAL MODEL

We use a one-dimensional approximation for the fluid mechanics in the electrode equivalent to that used to model the experiment in Section 3.2. We nondimensionalise the vertical velocity component w with the electrode velocity $U = 0{\cdot}5$ meters per day $\approx 6 \times 10^{-6}$ m sec^{-1}, and the vertical distance z with the characteristic length scale

$$L = \sqrt{\frac{2\mathcal{M}_2 U}{\rho_2 g}}, \tag{51}$$

where $\mathcal{M}_2$ is a typical value of the temperature-dependent paste viscosity μ_2.

We seek a steady state so that the equations of motion reduce to

$$\alpha w = -Q, \qquad (\bar{\mu}_2 \alpha w_z)_z = \alpha, \tag{52}$$

where Q, the flux of paste, is a constant, as yet unknown. At the top $z = 0$ of the electrode the stress is assumed to be zero and the void fraction α is prescribed, so that

$$\alpha(0) = \alpha_0, \qquad w_z(0) = 0. \tag{53}$$

At some point $z = -b$ say, the paste becomes baked solid and is therefore constrained to move with the imposed electrode speed U. Thus

$$w(-b) = -1. \tag{54}$$

The boundary conditions (53–54) enable us in principle to solve the second-order ordinary differential equation (52b) and then to find the constant Q. To do so, however, we need to know the functional form of $\bar{\mu}_2(z)$, which in general entails solving the coupled electrical and heat-transfer problems. Some insight into the behaviour to be expected is gained by considering the following simplified case. Suppose that the briquettes remain solid at the top of the electrode until they reach a point $z = -m$ where they melt. Thereafter they have a constant viscosity until they reach the baking point $z = -b$, at which point they become solid once more. The problem then reduces to

$$\begin{aligned} &\alpha = -Q/w, \qquad w(w_z/w)_z = 1, \qquad -b < z < -m, \\ &w_z = -m, \quad \alpha = \alpha_0, \quad z = -m, \\ &w = -1, \quad z = -b, \end{aligned} \tag{55}$$

the length of the melting zone being given by $l = b - m$. The form of the solution of (55) depends on the relative sizes of l and the length m of the unmelted zone. For $m > l + \sqrt{2}$,

$$w = -\frac{\sinh^2\left(D + \frac{(z+b)\sinh D}{\sqrt{2}}\right)}{\sinh^2 D}, \tag{56}$$

where the constant D is the unique strictly positive solution of

$$\sinh(2D + \sqrt{2}l \sinh D) = \sqrt{2}m \sinh D. \tag{57}$$

For $0 \leqslant m < l + \sqrt{2}$, the solution is

$$w = -\frac{\cos^2\left(D - \frac{(z+b)\cos D}{\sqrt{2}}\right)}{\cos^2 D}, \tag{58}$$

where D satisfies

$$\sin(2D - \sqrt{2}l \cos D) = \sqrt{2}m \cos D. \tag{59}$$

For the solution to be bounded, D must lie in the range $D^* \leqslant D < \pi/2$, where D^* is the unique root in $[0, \pi/2]$ of

$$\sqrt{2}D^* \sec D^* = l, \tag{60}$$

and $D = D^*$ corresponds to $m = 0$. With D constrained to lie in $[D^*, \pi/2)$, (59) has a unique solution. Finally, in the special case $m = l + \sqrt{2}$, the solution is simply

$$w = -\left(1 + \frac{(z+b)}{\sqrt{2}}\right)^2. \tag{61}$$

The main item of interest as far as the practical electrode production process is concerned is of course the 'baked-in' volume fraction α_b which determines whether or not the briquette-produced electrode is of sufficient strength and electrical conductivity. This is given by

$$\frac{\alpha_b}{\alpha_0} = -w(-m). \tag{62}$$

D may be eliminated from this expression to obtain a relationship between α_b/α_0 and the two parameters l and m:

$$l = \frac{\cos^{-1}\sqrt{\frac{\alpha_0}{\alpha_b}\left(1 - \frac{m^2\alpha_0}{2\alpha_b}\right)} - \sin^{-1}\sqrt{\frac{m^2\alpha_0}{2\alpha_b}}}{\sqrt{\frac{\alpha_0}{2\alpha_b}\left(1 - \frac{m^2\alpha_0}{2\alpha_b}\right)}} \quad \text{for } m < \sqrt{\frac{2\alpha_b}{\alpha_0}}, \tag{63}$$

$$l = \frac{\cosh^{-1}\sqrt{\frac{m^2\alpha_0}{2\alpha_b}} - \sinh^{-1}\sqrt{\frac{\alpha_0}{\alpha_b}\left(\frac{m^2\alpha_0}{2\alpha_b} - 1\right)}}{\sqrt{\frac{\alpha_0}{2\alpha_b}\left(\frac{m^2\alpha_0}{2\alpha_b} - 1\right)}} \quad \text{for } m > \sqrt{\frac{2\alpha_b}{\alpha_0}}, \tag{64}$$

$$l = \sqrt{2}\left(\sqrt{\frac{\alpha_b}{\alpha_0}} - 1\right) \quad \text{for } m = \sqrt{\frac{2\alpha_b}{\alpha_0}}. \tag{65}$$

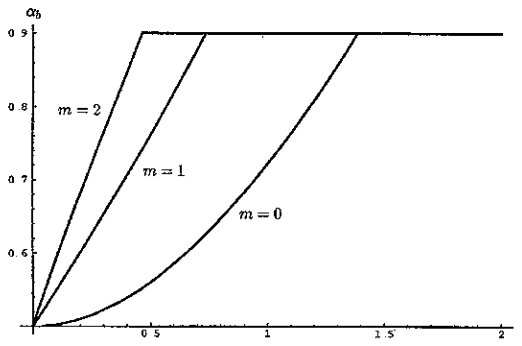

Figure 9. Baked-in paste volume fraction α_b versus length of the melted zone l, for various values of the length of the unmelted zone m. Here $\alpha_0 = 0.5$, $\alpha_c = 0.9$

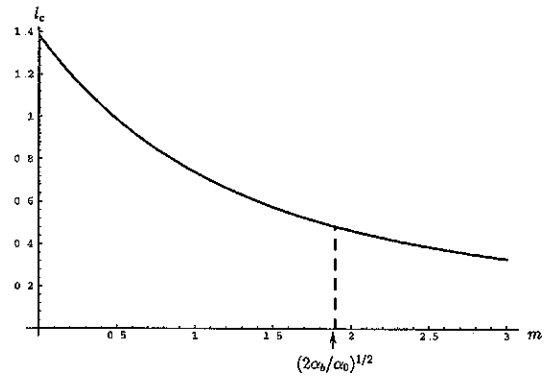

Figure 10. Critical length l_c of the melted zone, above which the maximum possible paste volume fraction is achieved, versus length m of the unmelted zone. Here $\alpha_0 = 0.5$, $\alpha_c = 0.9$. The dotted line shows point of transition between the two different solutions.

On physical grounds, we anticipate that the baked-in volume fraction α_b should be an increasing function of both m (which is effectively the weight pushing down on the melted zone) and the length of the melted zone l. However, the expressions (63)–(65) are only valid for $\alpha_b \leqslant \alpha_c$, where α_c is the maximum possible value of α defined earlier. If α reaches α_c at any point in the electrode (above the baking zone), then it remains at that value thereafter. We denote by l_c the critical value of l such that α_b first equals α_c at $l = l_c$. Then, if l is increased past l_c, (63)–(65) cease to apply and α_b simply remains at the value α_c.

We plot α_b against l in Figure 9, for various values of m, using the parameter values $\alpha_0 = 0.5$ and $\alpha_c = 0.9$. In order to maximise the strength of the baked electrode, it is desirable to make α_b as large as possible. In order to do so, one should ensure that $l > l_c$, so that α_b is at its maximum value of α_c. We plot l_c versus m in Figure 10, for the same values of α_0 and α_c. The dotted line shows the transition between solutions (63) and (64).

Because of the gross simplifying assumptions made regarding the viscosity, the results of this simple model of the Persson electrode should be regarded as merely qualitative. Nevertheless, they provide some insight into the process of manufacturing briquette-charged electrodes.

6. Conclusions and discussion

The theory developed above has shown that the briquette-squashing experiment may be modelled successfully using the two-phase slow flow equations. More data is required regarding the effects of temperature variation, but the agreement between the predictions and the experimental results is encouraging. Whilst our consideration of the future for briquette-charged Persson and Bruff electrodes is incomplete, it has been shown that it is possible to determine most of the qualitative details of the processes. Although numerical work is required for real electrodes, there seems to be no reason why the development of practical predictive tools should not be possible in the near future. In particular, it should be stressed that a careful two-phase flow approach is necessary, since by formulating the models carefully from first principles the approximations inherent in the equations can be clearly enunciated.

In both the experimental and industrial cases analysis has shown that a number of different regimes will probably be present. Different problems must be solved in each regime. The regimes considered above actually represent a simplification of the real situation, since no account has been taken so far of what happens in the final stages of the briquette recharging of electrodes when the pores in the melting paste close and air can no longer escape. This is likely to lead to complicated and involved modelling, but is probably unlikely to affect predictions materially. In any case, the important time scales for both the experiment and the industrial electrode may be obtained.

Whilst little attention has been given to the Bruff electrode, where the paste is melted and baked by heating provided by propane burners and the combustion of escaping paste hydrocarbons, it is clear that an inherent optimisation problem arises. If the heaters are not hot enough then an electrode with low strength and electrical conductivity will be produced. However, if the temperature of the heaters is too high, not only will energy be wasted, but there is a danger of creating 'baked in' voids in the electrode. A model similar to that developed for the Persson electrode may well prove to be an important manufacturing optimisation tool if briquette charging is to be used for electrode replenishment.

Finally, we anticipate that the feasibility of briquette charging for other electrode designs could be analysed, using techniques similar to those developed here.

Appendix: Solution of free-boundary problems

Consider the system of partial differential equations

$$\alpha_t + (\alpha w)_z = 0, \qquad (\alpha w_z)_z = g^*\alpha, \tag{A1}$$

with boundary conditions

$$\begin{aligned} &\alpha = \alpha_0, \qquad s = 1, \quad t = 0, \\ &w = 0, \quad z = 0, \\ &\alpha w_z = -1, \qquad w = \dot{s}, \quad z = s(t). \end{aligned} \tag{A2}$$

Here the initial volume fraction α_0 is a given constant. Interestingly, if g^* is negative, the same free-boundary problem governs the extension under gravity of a fibre (with α identified with the cross-sectional area) or two-dimensioanl sheet (with α identified with the thickness) of viscous liquid – see for example [10]. In such an application, the boundary condition (A2,c) on $z = s(t)$ corresponds to a compressive force applied to the free end (*e.g.* surface tension). The more general case in which α is spatially nonuniform initially and (A2,c) becomes $[\alpha w_z]_{z=s(t)} = f(t)$ is also readily tackled by the methods shown below.

We transform to Lagrangian variables defined via $(x, t) \to (\xi, \tau)$ where

$$z = Z(\xi, \tau), \qquad t = \tau, \qquad \frac{\partial Z(\xi, \tau)}{\partial \tau} = w(Z(\xi, \tau), t), \qquad Z(\xi, 0) = \xi. \tag{A3}$$

Once (A1,a) is transformed according to (A3), it may be integrated once to give

$$\alpha Z_\xi = \alpha_0. \tag{A4}$$

Using (A4), we may reduce (A1,b) to

$$\alpha_{\xi\tau} = -g^*\alpha_0, \tag{A5}$$

and hence

$$\alpha = \alpha_0 + g^*\alpha_0\tau(1-\xi) + \tau. \tag{A6}$$

Finally, substituting (A6) in (A4) and integrating, we obtain

$$Z(\xi,\tau) = \int_0^\xi \frac{\alpha_0\,\mathrm{d}\xi'}{\alpha_0 + g^*\alpha_0\tau(1-\xi) + \tau}. \tag{A7}$$

In general, combining (A6) and (A7) gives a parametric description of α as function of z for each t. From this we can also deduce the length s:

$$s(t) = Z(1,t). \tag{A8}$$

Since in our case $\alpha_0 = \text{const.}$, (A7) is easily inverted to give ξ as a function of z and t, and thus explicit formulae for $\alpha(z,t)$ and $s(t)$ are obtained.

The solution (A6) allows α to grow without bound. We suppose that this continues until α reaches some critical value α_c, after which α remains at that value and the paste ceases to flow. Since we have taken $\alpha_0 = \text{const.}$, this must first occur at $z = 0$, $t = t_c$, where

$$t_c = \frac{\alpha_c - \alpha_0}{1 + \alpha_0 g^*}.$$

(For arbitrary spatially-varying α_0, the situation is potentially much more complicated, since it is possible for 'pockets' in which $\alpha = \alpha_c$ to open up in the interior of the fluid domain.) For $t > t_c$, the boundary condition (A2,b) is replaced by

$$\alpha = \alpha_c, \qquad w = 0, \qquad z = l(t),$$

with also the conditions (A2,c) on $z = s(t)$.

The Equation (A6) for α remains valid so long as the paste continues to flow. The critical value $\alpha = \alpha_c$ occurs at $\xi = \lambda(\tau)$, where

$$\lambda(\tau) = \frac{(1 + g^*\alpha_0)\tau - (\alpha_c - \alpha_0)}{g^*\alpha_0\tau}.$$

Now the general form for Z is

$$Z(\xi,\tau) = Z_0(\tau) + \int_0^\xi \frac{\alpha_0\,\mathrm{d}\xi'}{\alpha_0 + g^*\alpha_0\tau(1-\xi) + \tau}.$$

The function Z_0 is determined from the initial-value problem

$$Z_{0\tau}(\lambda(\tau),\tau) = 0, \qquad Z_0(t_c) = 0. \tag{A9}$$

Then, as before, we have a parametric description of α as a function of z which is readily inverted to give $\alpha(z, t)$ explicitly.

For the case of temporally-varying viscosity, we simply note that the equations and boundary conditions are reduced to those for constant viscosity after the transformation

$$t^* = F(t) = \int_0^t \frac{\mathrm{d}t'}{\bar{\mu}_2(t')}, \qquad w^* = \bar{\mu}_2 w. \tag{A10}$$

Acknowledgements

The authors are grateful to Svenn Anton Halvorsen of Elkem ASA, Kristiansand, Norway who first brought this problem to our attention at the 1997 Study Group with Industry, University of Bath. They also recognise the contribution of other members of the group that worked on this problem at the meeting. PDH was funded by a Junior Research Fellowship from Christ Church College, Oxford.

References

1. R. Innvaer, A status for the Søderberg smelting electrode. UIE, Electrotech 92, Montreal (1992).
2. D. A. Drew and R. T. Wood, *Overview and Taxonomy of Models and Methods for Workshop on Two-phase Flow Fundamentals* National Bureau of Standards, Gaithersburg, Maryland (1985).
3. D. A. Drew, Mathematical modelling of two-phase flow. *Ann. Rev. Fluid Mech.* 15 (1983) 261–291.
4. A. D. Fitt, Mixed systems of conservation laws in industrial mathematical modelling *Surv. Math. Ind.* 6 (1996) 21–53
5. K. Tørklep, Viscometry in paste production. *Light Metals* Proc. Sess. AIME Annu. Meet. 117th (1988) 237–244.
6. S. Kakac and Y. Yener, *Convective Heat Transfer* (2nd. edn) CRC Press (1995) 483pp.
7. C. F. Fulgenzi, New electrodes for arc furnaces. *Proc. ABM Conf.* Vitoria, Brazil (1992)
8. J. A. Persson and N. G. Fava, Silicon furnace technology. *AIME Electric Furnace Conf. Proceedings*, 49 Toronto, Canada (1991) 186–194.
9. C. J. Budd, *Proceedings of the 1997 European Study Group with Industry*. University of Bath (1997).
10. J. N. Dewynne, P. D. Howell and P. Wilmott, Slender viscous fibres with inertia and gravity. *Quart. J. Mech. Appl. Math.* 47 (1994) 541–555